ACS APPLIED MATERIALS & INTERFACES

Research Article

www.acsami.org

Microemulsion-Assisted Synthesis of Mesoporous Aluminum Oxyhydroxide Nanoflakes for Efficient Removal of Gaseous Formaldehyde

Zhihua Xu,[†,‡,§] Jiaguo Yu,*[,†] Jingxiang Low,[†] and Mietek Jaroniec*[,‡]

[†]State Key Laboratory of Advanced Technology for Materials Synthesis and Processing, Wuhan University of Technology, Wuhan 430070, P. R. China

[‡]Department of Chemistry, Kent State University, Kent, Ohio 44242, United States

[§]College of Chemical Engineering, Huanggang Normal University, Huanggang 438000, P. R. China

Supporting Information

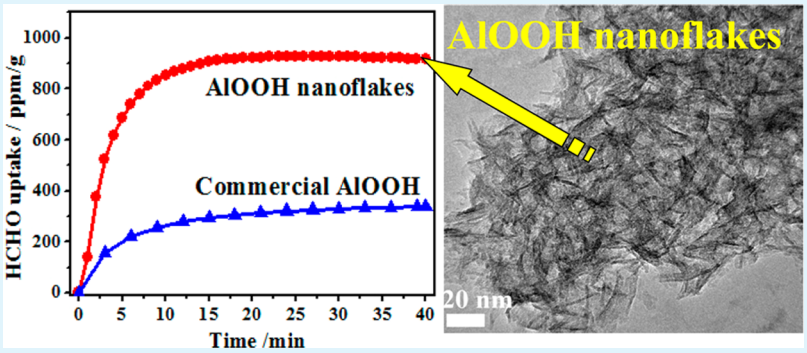

ABSTRACT: Mesoporous aluminum oxyhydroxides composed of nanoflakes were prepared via a water-in-oil microemulsion-assisted hydrothermal process at 50 °C using aluminum salts as precursors and ammonium hydroxide as a precipitating agent. The microstructure, morphology, and textural properties of the as-prepared materials were characterized by X-ray diffraction (XRD), transmission electron microscopy (TEM), Fourier transform infrared spectroscopy (FTIR), nitrogen adsorption, and X-ray photoelectron spectroscopy (XPS) techniques. It is shown that the aluminum oxyhydroxide nanostructures studied are effective adsorbents for removal of formaldehyde (HCHO) at ambient temperature, due to the abundance of surface hydroxyl groups, large specific surface area, and suitable pore size. Also, the type of aluminum precursor was essential for the microstructure formation and adsorption performance of the resulting materials. Namely, the sample prepared from aluminum sulfate (Al-s) exhibited a relatively high HCHO adsorption capacity in the first run, while the samples obtained from aluminum nitrate (Al-n) and chloride (Al-c) exhibited high adsorption capacity and relatively stable recyclability. A combination of high surface area and strong surface affinity of the prepared aluminum oxyhydroxide make this material a promising HCHO adsorbent for indoor air purification.

KEYWORDS: *aluminum (oxy)hydroxide, mesoporous materials, adsorption, formaldehyde removal*

1. INTRODUCTION

Recently, considerable attention has been directed to the environmental problems involving indoor air cleaning. Formaldehyde (HCHO), as one of the dominant air pollutants in indoor environment, can cause adverse effects on human health. Many technologies including physical adsorption and catalytic oxidation have been proposed for the removal of HCHO.[1−5] Among them, physical adsorption has advantages in terms of low cost and easy operation. A number of adsorbents, such as SiO_2,[6] Al_2O_3,[7] CeO_2,[8] MgO,[9] TiO_2,[10] $KMnO_4$, and activated carbon (AC),[11−13] have been studied for eliminating gaseous HCHO. However, the performance of the aforementioned adsorbents is not satisfactory due to their low adsorption capacity and/or difficult regeneration. Thus, recent efforts have been focused on the design of novel inexpensive adsorbents with high adsorption capacity.[14−17] It is generally recognized that the state of HCHO on the adsorbent surface plays a vital role in the adsorption process, which mainly depends on the degree of surface affinity, surface area and pore size distribution. Considering HCHO is a typically hydrophilic and polar molecule, it is desirable to develop novel adsorbents with a hydrophilic nature, large surface area, and suitable pores for HCHO adsorption.

Received: November 19, 2013
Accepted: January 13, 2014
Published: January 13, 2014

Recently, the development of mesoporous structures with designed surface functionality and unique morphology has attracted tremendous interest due to their potential applications in catalysis, adsorption, separation, and controlled drug delivery and release.[18−21] Among mesoporous materials, the nanostructured aluminum (oxy)hydroxides have been explored in a wide range of applications such as adsorbents, catalyst supports, catalyst promoters, and precursors for production of alumina,[21−24] many of which depend on the morphological and structural features such as shape, surface area, and pore/particle size.[25−27] Up to now, various morphologies of aluminum oxyhydroxide have been prepared such as spindle-like,[25] flower-like,[24,29] cantaloupe-like,[30] nanowires,[31] hollow core/shell and microspheres,[32] nanotubes, and nanorods.[33] Often, aluminum oxyhydroxide was prepared via hydrothermal or solvothermal processes under high pressure in a sealed autoclave at relatively high temperatures (above 100 °C), in which different additives such as sodium tartrate, sodium amide, and trisodium citrate were used to control its morphology. Moreover, these high-temperature preparation processes afforded aluminum oxyhydroxide with higher crystallinity, but relatively low specific surface area. An attractive strategy for the synthesis of nanomaterials is a microemulsion-based method, which enables one to control their properties such as particle size, morphology, surface area, and homogeneity.[34,35] Herein, we used a microemulsion-assisted hydrothermal method at a relatively low temperature (50 °C) to prepare aluminum oxyhydroxides with high specific surface area, which is an important factor for achieving high concentration of active sites for adsorption. Previous studies showed that hierarchical boehmite is an efficient adsorbent for removal of Congo red, phenol, and Cr(VI) present in model wastewater.[32,36] However, to the best of our knowledge, aluminum (oxy)hydroxide nanoflakes with high specific surface area have not been investigated yet for adsorbing gaseous HCHO at ambient temperature. Moreover, as a typical layered material, γ-AlOOH is strongly hydrophilic because of the abundant amount of hydroxyl groups. Thus, the hydrophilic surface is well suited for adsorbing polar organic molecules via hydrogen bonding.

2. EXPERIMENTAL SECTION

2.1. Preparation. In a typical synthesis, a mixture containing 100 mL of cyclohexane and 20.46 g of polyethylene glycol (PEG 400) was magnetically stirred and heated to 50 °C. After stirring for 10 min at 50 °C, 20 mL of aluminum precursor (0.32 M Al) solution and 3.50 g of NH_3 solution (27 wt %) were added stepwise to the above solution, and then aged for 8 h to allow hydrolysis of aluminum precursor. At the end of each synthesis, about 30 mL of isopropanol was added to the mixture to destabilize the microemulsion structure. The obtained mixture was separated by centrifugation, and the resulting hydrogel was washed four times with deionized water, then two times with ethanol, and finally dried overnight at ca. 65 °C in a vacuum oven and at 80 °C for about 30 min.

The final white xerogel samples were labeled, starting with a prefix of Al followed by the type of aluminum precursors (s, n, and c, which refer to aluminum sulfate, aluminum nitrate, and aluminum chloride, respectively). For example, Al-s refers to an aluminum oxyhydroxide prepared from aluminum sulfate. For the purpose of comparison, two commercial samples of AlOOH and active carbon, denoted as c-AlOOH and c-carbon, respectively, were studied.

2.2. Characterization. The phase structure and morphology of the samples were analyzed on a Philips X'Pert X-ray diffractometer (XRD) using Cu Kα radiation (λ = 0.15419 nm) and on a JEM-2100F transmission electron microscope (TEM) (JEOL, Japan). X-ray photoelectron spectroscopy (XPS) measurements were performed on an ESCALAB250xi spectrometer (Thermon Scientific). All the binding energies were referenced to the C1s peak at 285 eV. Nitrogen adsorption−desorption isotherms were obtained on an ASAP 2020 (Micromeritics Instruments) gas adsorption apparatus. All the samples were degassed at 100 °C prior to adsorption measurements. The Brunauer−Emmett−Teller (BET) surface area (S_{BET}) was determined by a multipoint BET method by using adsorption data in the relative pressure P/P_0 range of 0.05−0.2. The single-point pore volume (V_p) was estimated from the amount adsorbed at a relative pressure of 0.98. The pore size distributions (PSD) were calculated using adsorption branches of nitrogen adsorption-desorption isotherms by the improved KJS method.[27,37] Fourier transform infrared (FTIR) spectra were collected using a Shimadzu IRAffinity-1 FTIR spectrometer in a range of 4000−400 cm^{-1}.

2.3. HCHO Adsorption Tests. HCHO adsorption was performed in an organic glass box covered by a layer of aluminum foil on its inner wall at ambient temperature. 0.1 g of adsorbent was dispersed on the bottom of a glass petri dish having diameter of 14 cm. After placing the sample-contained dish in the bottom of reactor with a glass slide cover, a certain amount of condensed HCHO (38%) was injected into the reactor having a 5 W fan in the bottom of reactor. After 2−3 h, the HCHO solution was volatilized completely and the concentration of HCHO was stabilized. HCHO, CO_2, CO, and water vapor were on-line analyzed with a Photoacoustic IR multigas monitor (INNOVA air Tech Instruments model 1412). The HCHO vapor was allowed to reach adsorption/desorption equilibrium within the reactor prior to the experiment. The initial concentration of HCHO after adsorption/desorption equilibrium was controlled at ca. 150 ppm, which remained constant until the glass slide cover on the petri dish was removed to start HCHO adsorption. In the recycle experiments, the adsorbents were heated at 80 °C for ca. 15 min before next run of HCHO adsorption.

3. RESULTS AND DISCUSSION

TEM images of Al-s, Al-n, and Al-c are shown in Figure 1. These images reveal a porous microstructure composed of

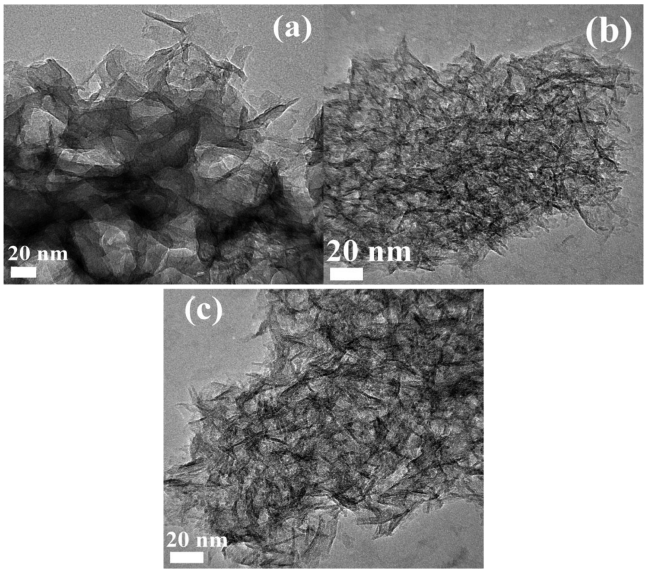

Figure 1. TEM images of Al-s (a), Al-n (b), and Al-c (c).

randomly aggregated and interconnected ca. 2 nm thick nanoflakes. The selected area electron diffraction patterns of all samples (see Supporting Information Figure S1) show broad diffraction rings, indicating that all the as-prepared samples are polycrystalline. Since the nanoflakes are heavily aggregated, their dimensions cannot be precisely evaluated by TEM. However, as compared to the previously reported AlOOH-silica

spheres,[36] the nanoflakes studied are much thinner and smaller. The formation of the ultrathin and small nanoflakes is attributed to the restricted growth of nanoflakes because of using PEG and microemulsion. PEG can be adsorbed preferably on the crystal plane of aluminum (oxy)hydroxide flakes via hydrogen bonding with the OH groups present on its surface. Adsorption of PEG molecules considerably restricts the growth along the aforementioned plane of the aluminum (oxy)hydroxide nanocrystals, which means that the nuclei grow in a two-dimensional (2D) mode to produce very thin nanoplates.[38] However, the nanoflake dimensions of Al-n and Al-c are observed to be similar, distinctly smaller than that of Al-s. In the preparation process, an excessive amount of NH_3 results in the negative charge of aluminum (oxy)hydroxide colloid in the microemulsion. Due to the weaker coagulation ability of SO_4^{2-} than NO_3^- and Cl^- anions, originated from its larger negative charge number, the negatively charged aluminum (oxy)hydroxide nanoflakes can grow larger before the coagulation in the solution containing SO_4^{2-} anions than those in the solution containing NO_3^- and Cl^- anions. Therefore, the nanoflakes of Al-s are larger than those of Al-n and Al-c. Furthermore, no obvious discrepancies are observed between the nanoflakes obtained from $Al(NO_3)_3$ and $AlCl_3$, indicating a small difference in the effect of NO_3^- and Cl^- on the morphology of the as-prepared samples, which is consistent with the previous report.[28] As expected, Al-s sample exhibited the larger pore diameter due to the larger size of nanoflakes. Moreover, Al-s showed a more open structure than those of Al-n and Al-c, which can facilitate diffusion of molecules into the interior space of the adsorbent. The above result indicates the influence of aluminum precursor on the structure of the as-prepared samples.

Wide-angle XRD was used to identify the phase structures of the samples prepared from different precursors (as shown in Figure 2). All the detectable peaks in commercial AlOOH (c-AlOOH) can be assigned to orthorhombic γ-AlOOH (JCPDS No. 21-1307). Al-n and Al-c exhibit similar XRD patterns to commercial AlOOH, and all the diffraction peaks can be also indexed to γ-AlOOH (JCPDS No. 21-1307); their intensities are much weaker than those of the commercial AlOOH, indicating poor crystalline structure and/or smaller size of crystallites. Moreover, no characteristic peaks from other phase are observed, indicating high purity of the resulting samples. However, Al-s shows a distinct difference in the diffraction pattern at ca. 10−25°/2θ, which in this case is a combination of patterns of Boehmite (JCPDS No.74-1895) and Bayerite (JCPDS No. 38-0376; marked by an asterisk (*)). The observed difference in the XRD patterns may be attributed to the higher affinity of SO_4^{2-} than that of NO_3^- or Cl^-.[28] Due to the strong affinity of SO_4^{2-} to the bridged polymeric hydroxylated aluminum complexes, the newly formed $Al(OH)_3$ is more stable, and the subsequent conversion to γ-AlOOH is delayed at the same preparation time. So, the Al-s sample is a mixture of AlOOH and $Al(OH)_3$ phases. The average crystallite sizes of Al-c and Al-n estimated by Scherrer formula using the (200) peak are 6.1 and 7.0 nm, respectively; and the crystallite size of Al-s evaluated by the same formula using the (002) peak is 6.1 nm. It is anticipated that anions can influence the phase structure and crystallite size of aluminum (oxy)hydroxide, and consequently its performance for adsorption-based removal of HCHO from air.

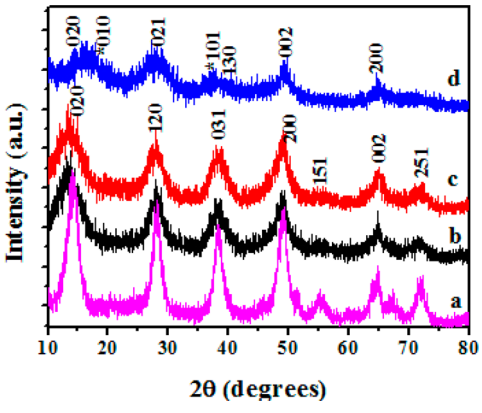

Figure 2. XRD patterns of c-AlOOH (a), Al-c (b), Al-n (c), and Al-s (d).

The FTIR spectra of Al-s, Al-n, and Al-c are shown in Figure 3. As can be seen from the spectra, the surfaces of all the samples are highly hydroxylated, as evidenced by an intense and broad peak at 3100−3700 cm^{-1} assigned to the stretching vibration of OH (Al and/or tunnel water species). A wide range of the absorption band can be attributed to the continuous distribution of chemical bond (of O−H) in ultrafine particles or amorphous structure.[39] The medium peaks at 1639 and 1072 cm^{-1} are assigned to the deformation vibration of adsorbed water and the bending vibration of Al−O−H, respectively.[31,33] The bands at 883 and 750 cm^{-1} are related to the vibration mode of AlO_6.[40,41] A closer look at the FTIR spectra indicates that the three samples show some differences. Specifically, a strong band at ca. 1122 cm^{-1} and a small band at 619 cm^{-1} observed in the spectrum of Al-s are due to the vibration of residual sulfate ions in the sample. Two strong bands at ca. 2366 and 2330 cm^{-1} attributed to the vibration of CO_2 are observed in the spectrum of Al-s, and two similar moderate bands are visible in the spectrum Al-n, while no related peaks are observed in the case of Al-c. Moreover, a moderately intense band at ca. 1421 cm^{-1} in the spectrum of Al-s attributed to the symmetric stretching of adsorbed CO_2,[42] exhibits a high-wavenumber shift as compared with those (at ca. 1388 cm^{-1}) in the spectra of Al-n and Al-c. However, it has to be noted that the stronger band at ca. 1388 cm^{-1} in the spectrum of Al-n than that related to Al-c is also due to a partial contribution of some residual nitrate species. This phenomenon presumably indicates that the surface hydroxyl groups of Al-s and Al-n, especially in the case of Al-s, are more basic and active.

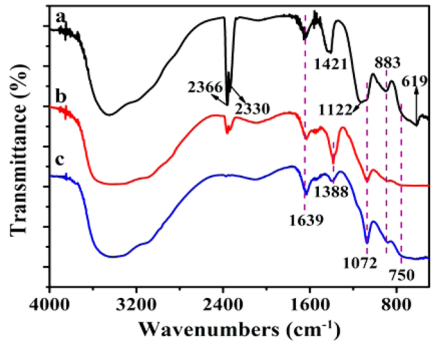

Figure 3. FTIR spectra of Al-s (a), Al-n (b), and Al-c (c).

Usually, adsorbents with high specific surface area, large pore volume and appropriate pore sizes perform well due to

significantly high number of surface active sites that enhance adsorption of adsorbate molecules and facilitate their diffusion into the interior of adsorbents. Therefore, the effect of the precursors on the pore structure and surface area of aluminum (oxy)hydroxide is investigated by N_2 adsorption-desorption measurements. Figure 4 shows the N_2 adsorption-desorption

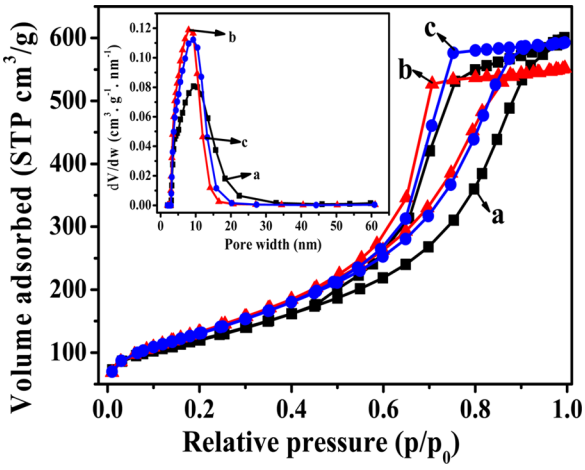

Figure 4. Nitrogen adsorption/desorption isotherms of Al-s (a), Al-n (b), and Al-c (c). The inset shows the corresponding pore size distribution expressed as the derivative of the pore volume with respect to the pore width.

isotherms and the corresponding pore size distribution curves (inset) of the samples studied. All the samples give type IV isotherms, reflecting the the presence of mesopores.[43] The Al-n and Al-c samples show H2-type hysteresis loops, which are associated with an interconnected pore network.[44] In comparison, Al-s shows a large H2-type hysteresis loop in the range of 0.45−0.9 P/P_0, suggesting the presence of an interconnected pore network, and a small H3-type hysteresis loop in the range of 0.9−1.0 P/P_0, indicating larger slit-like mesopores resulted from the aggregation of larger nanoflakes.[32,43] This result is consistent with TEM images. Moreover, the condensation step of the isotherm measured on Al-s shifts clearly toward higher P/P_0 as compared to those of Al-n and Al-c. This suggests that Al-s has larger mesopores than Al-n and Al-c, which can be further confirmed by the pore size distribution curves. The PSD curve calculated for Al-s is in the range of 3-33 nm with a peak located at the pore diameter of ~9.4 nm, while those obtained for Al-n and Al-c are located in narrower range (3-20 nm) with a peak at the pore diameters of 8.0 and 9.3 nm, respectively, further confirming the presence of mesopores. Table 1 shows the basic adsorption characteristics such as the BET surface area (S_{BET}), pore volume (V_p), and pore size width (d_p) at the maximum of PSD for the as-prepared aluminum (oxy)hydroxides, commercial AlOOH (c-AlOOH) and active carbon (c-carbon). The as-prepared samples exhibit larger specific surface areas (434−488 m^2/g) and pore volumes (0.85−0.92 cm^3/g) than the corresponding values of S_{BET} (84−443 m^2/g) and V_p (0.3−0.7 cm^3/g) available in literature,[29−33,36,45,46] indicating the advantage of the proposed synthesis method. Moreover, as can be seen from Table 1, Al-n has a specific surface area of 488 m^2/g, similar to Al-c (478 m^2/g) and higher than that of Al-s (434 m^2/g). Al-s exhibits the pore size of 9.4 nm, which is similar to that of Al-c (9.30 nm) and larger than that of Al-n (7.98 nm), and the pore volume of 0.91 cm^3/g, similar to that of Al-c (0.92 cm^3/g) and

Table 1. Physical Properties of the Samples[a]

samples	AC (ppm/g)	AC/S (ppm/m^2)	S_{BET} (m^2/g)	d_p (nm)	V_p (cm^3/g)
Al-s	1008	2.32	434	9.41	0.91
Al-n	880	1.80	488	7.98	0.85
Al-c	907	1.90	478	9.30	0.92
c-AlOOH	344	1.11	310	3.08	0.28
c-carbon	187	0.48	390	1.83	0.23

[a]AC, HCHO adsorption capacity in the first run; AC/S, HCHO adsorption capacity per specific surface area; S_{BET}, BET specific surface area; d_p, pore width at the maximum of the pore size distribution; and V_p, single-point pore volume.

larger than that of Al-n (0.85 cm^3/g). The smaller S_{BET} and larger V_p and d_p of Al-s are mainly attributed to larger dimensions of nanoflakes. The relatively larger mesopores and pore volume are expected to benefit the diffusion process. In addition, a closer look at the adsorption data shows that Al-c possesses larger outer and interior voids, which could accommodate a larger amount of guest molecules. The above results illustrate the effect of aluminum precursor on the textural parameters of the resulting aluminum (oxy)hydroxides. The differences in the porous structure among the samples studied may lead to different adsorption performance for removal of HCHO from air.

Figure 5 shows the high-resolution XPS O 1s spectra of Al-s, Al-n, and Al-c. The broad O 1s peaks of all the samples are

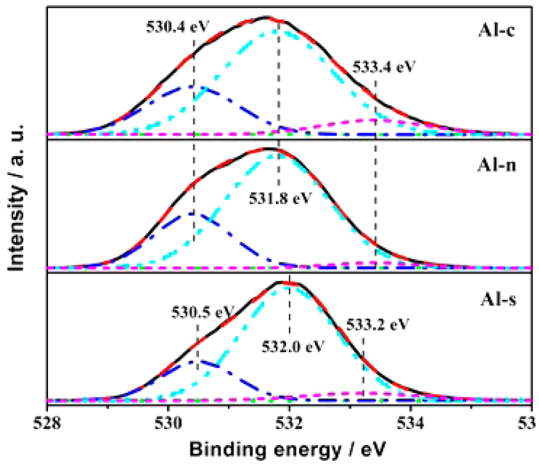

Figure 5. High-resolution XPS O 1s spectra of Al-s, Al-n, and Al-c.

deconvoluted into three contributions. The peaks at 530.4−530.5, 531.8−532.0, and 533.2−532.4 eV are attributed to oxygen in the crystal structure ($O_{crystal}$), hydroxyl (O_{OH}), and adsorbed water, respectively.[47,48] The ratios of O/Al (atom%), O_{OH}/O_{total}, and $O_{crystal}/O_{total}$ based on XPS analysis are listed in Table 2. The measured O/Al ratio for Al-s is 2.47; this value is between the theoretical data predicted for $Al(OH)_3$ and AlOOH, indicating that this sample is a mixture of $Al(OH)_3$ and AlOOH, which is in agreement with the XRD analysis. In

Table 2. XPS Analysis Results of the As-Synthesized Samples

samples	O/Al ratio (atom %)	O_{OH}/O_{total}	$O_{crystal}/O_{total}$
Al-s	2.47	74.4%	19.9%
Al-n	2.05	66.1%	24.9%
Al-c	2.00	71.0%	26.9%

dx.doi.org/10.1021/am405224u | ACS Appl. Mater. Interfaces 2014, 6, 2111−2117

contrast, the O/Al ratios obtained for Al-n and Al-c are very close to two, which is the theoretical O/Al ratio for AlOOH, further indicating that these samples mainly consisted of AlOOH. As can be seen from Figure 5 and Table 2, the deconvoluted peak corresponding to hydroxyl group is dominating, and larger than that related to O in the crystal structure, indicating an abundance of surface hydroxyls on all the samples. The active surface hydroxyls are beneficial to adsorption of gaseous formaldehyde. As can be seen from Table 2, Al-s exhibits 74.4% of surface hydroxyls, which is higher than the corresponding values for Al-c (71.0%) and Al-n (66.1%). A higher amount of surface hydroxyls will lead to a higher adsorption capacity towards HCHO.

Figure 6 shows HCHO uptakes as a function of time on c-carbon, c-AlOOH and the as-prepared samples. The HCHO

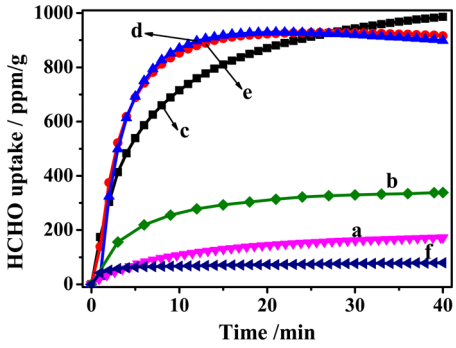

Figure 6. HCHO uptake as a function of time measured on c-carbon (a), c- AlOOH (b), Al-s (c), Al-n (d), Al-c (e), and hollow AlOOH (f).

adsorption on all the adsorbents is very rapid within initial 8 min and then gradually levels off, indicating the approach to equilibrium. The HCHO adsorption capacities of all the samples are listed in Table 1. The as-prepared adsorbents show much higher HCHO uptakes that are 1008 ppm/g for Al-s, 880 ppm/g for Al-n, and 907 ppm/g for Al-c, larger than those for c-AlOOH (344 ppm/g) and c-carbon (187 ppm/g). For the purpose of comparison, the hollow AlOOH microspheres (hollow AlOOH) showed a HCHO uptake of less than 80 ppm/g, mainly due to its smaller specific surface area (111 m^2/g) and smaller hydropilicity.[49] In order to investigate the effect of S_{BET} on the adsorption performance, we compared the HCHO adsorption capacity per unit surface area for all the adsorbents (see Table 1). This comparison indicates that this value is equal to 2.32 ppm/m^2 for Al-s and it is larger than the corresponding values for Al-c (1.90 ppm/m^2) and Al-n (1.80 ppm/m^2). In addition, the aforementioned values are much higher than those obtained for c-AlOOH and c-carbon. It is generally known that the adsorption performance of an adsorbent depends on its porous structure (specific surface area, pore size, and porosity volume), chemical properties, and surface affinity. Because of the high specific surface area, pore volume, plenty of surface hydroxyls, and suitable pore size, the as-prepared samples exhibited an excellent performance for HCHO adsorption.

Favorable adsorption of HCHO on the as-prepared aluminum (oxy)hydroxide is controlled by hydrogen bonding between HCHO and hydroxyl groups, which play a key role in this process.[23] Adsorption of HCHO on aluminum oxy-hydroxide is favored because of abundance of hydroxyl groups on the surface of this material,[50] which attract hydrophilic formaldehyde molecules via hydrogen bonding. Our previous studies showed that active hydroxyl groups can greatly enhance adsorption capacity of HCHO.[16,17] Therefore, the as-prepared aluminum (oxy)hydroxides with large specific surface area and large amount of surface hydroxyls exhibited an outstanding adsorption performance for HCHO. The HCHO uptake obtained for Al-s is higher than those for Al-n and Al-c, which correlates with the amount of surface hydroxyls; Al-c shows a slightly higher HCHO uptake than that for Al-n, which is also due to its higher amount of surface hydroxyls. Moreover, Al-s exhibited a slower rate of HCHO adsorption than the initial rates for Al-n and Al-c. Also, its HCHO adsorption capacity continued to slightly increase at the end of the measurement, while those obtained for Al-n and Al-c decrease at the same time period. Therefore, it is reasonable to assume that the HCHO adsorption on the Al-s is partly accompanied by a chemical adsorption process with a longer equilibrium time because of the high activity of some surface hydroxyls as indicated by the presence of strong CO_2 adsorption peaks on the FTIR spectra; however, adsorption of HCHO on Al-c or Al-n is mainly governed by physical interactions with a short equilibrium time, which is additionally confirmed by the subsequent recycling experiments.

To further compare the stability of the as-prepared adsorbents, a series of repetitive adsorption experiments was performed on a given sample at the same initial HCHO concentration, ca. 150 ppm. As shown in Figure 7, the HCHO

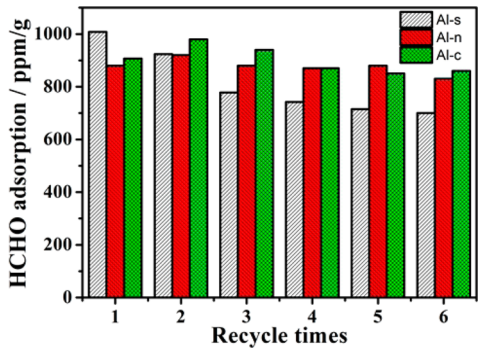

Figure 7. Comparison of HCHO adsorption with recycle times over Al-s, Al-n, and Al-c samples.

adsorption capacity of Al-s decreased during the initial two consecutive runs, mainly due to partially irreversible adsorption bonding and/or a partial loss of partial surface hydroxyls. In the case of Al-c, a slight increase was observed at the second run followed by a slight decrease in the following runs; however, a relatively stable HCHO adsorption capacity was recorded in the case of Al-n for all repetitive runs. Furthermore, similar HCHO adsorption capacities of Al-c and Al-n were recorded in the subsequent runs, which are higher than those obtained for Al-s. Also, the HCHO adsorption capacities of all the samples are relatively stable for the latter cycles, suggesting that the materials studied can be efficiently reused. The proposed facile synthesis of mesoporous aluminum (oxy)hydroxide adsorbents and their excellent adsorption performance and easy recovery indicate that these nanomaterials have a great potential for air purification.

dx.doi.org/10.1021/am405224u | ACS Appl. Mater. Interfaces 2014, 6, 2111−2117

4. CONCLUSIONS

Mesoporous aluminum (oxy)hydroxides were prepared by a water-in-oil microemulsion-assisted hydrothermal method at a relatively low temperature. The as-prepared nanoflakes showed a remarkable adsorption performance toward gaseous HCHO due to their mesoporous structure and abundant amount of surface hydroxyls. This study shows that the type of aluminum precursor has a pronounced effect on the porous structure of the adsorbents studied and their performance in removing HCHO from air. Al-s prepared from aluminum sulfate exhibited higher HCHO adsorption capacity in the first run, while the Al-n and Al-c prepared from aluminum nitrate and chloride respectively, exhibited better recyclability, which is mainly related to the mesoporous structure, surface hydroxylation and high specific surface area. This study demonstrates that the mesoporous aluminum (oxy)hydroxide with high specific surface area and plenty of surface hydroxyls can act as promising adsorbents for quick removal of indoor HCHO pollutant under ambient conditions.

■ ASSOCIATED CONTENT

Ⓢ Supporting Information

Additional TEM images of Al-s, Al-n, and Al-c. This material is available free of charge via the Internet at http://pubs.acs.org.

■ AUTHOR INFORMATION

Corresponding Authors

*E-mail: jiaguoyu@yahoo.com. Fax: +86 27 87879468. Tel: +86 27 87871029.

*E-mail: jaroniec@kent.edu. Fax: +1 330 672 3816. Tel: +1 330 672 3790.

Notes

The authors declare no competing financial interest.

■ ACKNOWLEDGMENTS

This work was partially supported by the 863 Program (2012AA062701), 973 Program (2013CB632402), NSFC (21307038, 51072154, 21177100, and 51272199), Key Project of Chinese Ministry of Education (212115), and PSFC (2012M521482 and 2013T60754).

■ REFERENCES

(1) Matsuo, Y.; Nishino, Y.; Fukutsuka, T.; Sugie, Y. *Carbon* **2008**, *46*, 1159−1174.
(2) Zhou, P.; Zhu, X.; Yu, J. G.; Xiao, X. *ACS Appl. Mater. Interfaces* **2013**, *5*, 8165−8172.
(3) Yu, J. G.; Li, X. Y.; Xu, Z. H.; Xiao, W. *Environ. Sci. Technol.* **2013**, *47*, 9928−9933.
(4) Yu, X.; He, J.; Wang, D.; Hu, Y.; Tian, H.; He, Z. *J. Phys. Chem. C* **2012**, *116*, 851−860.
(5) Nie, L. H.; Yu, J. G.; Li, X. Y.; Cheng, B.; Liu, G.; Jaroniec, M. *Environ. Sci. Technol.* **2013**, *47*, 2777−2783.
(6) Saeung, S.; Boonamnuyvitaya, V. *J. Environ. Sci.* **2008**, *20*, 379−384.
(7) Gao, H.; He, H.; Zhang, C.; Yan, T. *J. Mol. Struct.* **2008**, *891*, 242−246.
(8) Zhou, J.; Mullins, D. R. *Surf. Sci.* **2006**, *600*, 1540−1546.
(9) Xu, Y. J.; Zhang, Y. F.; Lu, N. X.; Li, J. Q. *Phys. B* **2004**, *348*, 190−197.
(10) Idriss, H.; Kim, K. S.; Barteau, M. A. *Surf. Sci.* **1992**, *262*, 113−127.
(11) Sekine, Y.; Nishimura, A. *Atmos. Environ.* **2001**, *35*, 2001−2007.
(12) Boonamnuayvitaya, V.; Sae-ung, S.; Tanthapanichakoon, W. *Sep. Purif. Technol.* **2005**, *42*, 159−168.
(13) Song, Y.; Qiao, W.; Yoon, S.; Mochida, I.; Guo, Q.; Liu, L. *J. Appl. Polym. Sci.* **2007**, *106*, 2151−2157.
(14) Carter, E. M.; Katz, L. E.; Speitel, G. E.; Ramirez, D. *Environ. Sci. Technol.* **2011**, *45*, 6498−6503.
(15) Ma, C.; Li, X.; Zhu, T. *Carbon* **2011**, *49*, 2869−2877.
(16) Xu, Z. H.; Yu, J. G.; Xiao, W. *Chem.—Eur. J.* **2013**, *19*, 9592−9598.
(17) Xu, Z. H.; Yu, J. G.; Liu, G. *Dalton Trans.* **2013**, *42*, 10190−10197.
(18) Deng, Y.; Cai, Y.; Sun, Z.; Liu, J.; Liu, C.; Wei, J.; Li, W.; Liu, C.; Wang, Y.; Zhao, D. *J. Am. Chem. Soc.* **2010**, *132*, 8466−8473.
(19) Angelos, S.; Johansson, E.; Stoddart, J. F.; Zink, J. I. *Adv. Funct. Mater.* **2007**, *17*, 2261−2271.
(20) Hu, S. H.; Liu, T. Y.; Huang, H. Y.; Liu, D. M.; Chen, S. Y. *Langmuir* **2008**, *24*, 239−244.
(21) Chang, F.; Zhang, M.; Wang, G.; Shi, W.; Hu, X. *Water, Air, Soil Pollut.* **2012**, *223*, 2073−2081.
(22) Yoon, T. H.; Johnson, S. B.; Brown, G. E., Jr. *Langmuir* **2005**, *21*, 5002−5012.
(23) Greathouse, J. A.; Hart, D. B.; Ochs, M. E. *J. Phys. Chem. C* **2012**, *116*, 26756−26764.
(24) Yu, X. X.; Yu, J. G.; Cheng, B.; Jaroniec, M. *J. Phys. Chem. C* **2009**, *113*, 17527−17535.
(25) Cai, W. Q.; Yu, J. G.; Mann, S. *Microporous Mesoporous Mater.* **2009**, *122*, 42−47.
(26) Cai, W. Q.; Yu, J. G.; Jaroniec, M. *J. Mater. Chem.* **2011**, *21*, 9066−9072.
(27) Cai, W. Q.; Yu, J. G.; Anand, C.; Vinu, A.; Jaroniec, M. *Chem. Mater.* **2011**, *23*, 1147−1157.
(28) Cai, W. Q.; Yu, J. G.; Jaroniec, M. *J. Mater. Chem.* **2010**, *20*, 4587−4594.
(29) Zhang, J.; Liu, S.; Lin, J.; Song, H.; Luo, J.; Elssfah, E. M.; Ammar, E.; Huang, Y.; Ding, X.; Gao, J.; Qi, S.; Tang, C. *J. Phys. Chem. B* **2006**, *110*, 14249−14252.
(30) Feng, Y.; Lu, W.; Zhang, L.; Bao, X.; Yue, B.; lv, Y.; Shang, X. *Cryst. Growth Des.* **2008**, *8*, 41426−41429.
(31) Zhang, J.; Wei, S.; Lin, J.; Luo, J.; Liu, S.; Song, H.; Elawad, E.; Ding, X.; Gao, J.; Qi, S.; Tang, C. *J. Phys. Chem. B* **2006**, *110*, 21680−21683.
(32) Cai, W. Q.; Yu, J. G.; Cheng, B.; Su, B. L.; Jaroniec, M. *J. Phys. Chem. C* **2009**, *113*, 14739−14746.
(33) Hou, H.; Xie, Y.; Yang, Q.; Guo, Q.; Tan, C. *Nanotechnology* **2005**, *16*, 741−745.
(34) Malik, M. A.; Wani, M. Y.; Hashim, M. A. *Arabian J. Chem.* **2012**, *5*, 397−417.
(35) López-Quintela, M. A. *Curr. Opin. Colloid Interface Sci.* **2003**, *8*, 137−144.
(36) Wang, Y.; Wang, G.; Wang, H.; Cai, W.; Liang, C.; Zhang, L. *Nanotechnology* **2009**, *20*, 155604−155610.
(37) Jaroniec, M.; Solovyov, L. *Langmuir* **2006**, *22*, 6757−6760.
(38) Wang, W.; Qiao, X.; Chen, J.; Li, H. *Mater. Lett.* **2007**, *61*, 3218−3220.
(39) Zou, J.; Dai, Y.; Tian, C.; Pan, K.; Jiang, B.; Wang, L.; Zhou, W.; Tian, G.; Wang, X.; Xing, Z.; Fu, H. *Environ. Sci. Technol.* **2012**, *46*, 4560−4566.
(40) Kong, J.; Chao, B.; Wang, T.; Yan, Y. *Powder Technol.* **2012**, *229*, 7−16.
(41) Gao, C.; Yu, X.; Xu, R.; Liu, J.; Huang, X. *ACS Appl. Mater. Interfaces* **2012**, *4*, 4672−4682.
(42) Bonelli, B.; Civalleri, B.; Fubini, B.; Ugliengo, P.; Areán, C. O.; Garrone, E. *J. Phys. Chem. B* **2000**, *104*, 10978−10988.
(43) Sing, K. S. W.; Everett, D. H.; Haul, R. A. W.; Moscou, L.; Pierotti, R. A.; Rouquerol, J.; Siemieniewska, T. *Pure Appl. Chem.* **1985**, *57*, 603−619.
(44) Sangwichien, C.; Aranovich, G. L.; Donohue, M. D. *Colloids Surf., A* **2002**, *206*, 313−320.
(45) Zhang, L.; Lu, W.; Cui, R.; Shen, S. *Mater. Res. Bull.* **2010**, *45*, 429−436.

(46) Zhang, L.; Lu, W.; Yan, L.; Feng, Y.; Bao, X.; Ni, J.; Shang, X.; Lv, Y. *Microporous Mesoporous Mater.* **2009**, *119*, 208−216.
(47) Kloprogge, J. T.; Duong, L. V.; Wood, B. J.; Frost, R. L. *J. Colloid Interface Sci.* **2006**, *296*, 572−576.
(48) Cruz, A. M. A.; Eon, J. G. *Appl. Catal., A* **1998**, *167*, 203−213.
(49) Cai, W. Q.; Yu, J. G.; Gu, S.; Jaroniec, M. *Cryst. Growth Des* **2010**, *10*, 3977−3982.
(50) Vatanpour, V. S; Madaeni, S.; Rajabi, L.; Zinadini, S.; Derakhshan, A. A. *J. Membr. Sci.* **2012**, *401-402*, 132−143.